2025 IEEE 9th Conference on Energy Internet and Energy System Integration (EI2) | 979-8-3315-4859-9/25/$31.00 ©2025 IEEE | DOI: 10.1109/EI268505.2025.11425441

Research on the Influencing Parameters for Target Operating Points and the Setting Principles of Controller Parameters

Jingao Ni
State Key Laboratory of Alternate Electrical Power System with Renewable Energy Sources North China Electric Power University
Beijing, China
120232201018@ncepu.edu.cn

Chongru Liu
State Key Laboratory of Alternate Electrical Power System with Renewable Energy Sources North China Electric Power University
Beijing, China
chongru.liu@ncepu.edu.cn

Hao Guo
State Key Laboratory of Alternate Electrical Power System with Renewable Energy Sources North China Electric Power University
Beijing, China
1245378131@qq.com

Yiming Tang
State Key Laboratory of Alternate Electrical Power System with Renewable Energy Sources North China Electric Power University
Beijing, China
tangym_0910@163.com

Yipeng Lv
State Key Laboratory of Alternate Electrical Power System with Renewable Energy Sources North China Electric Power University
Beijing, China
lvyipeng2000@ncepu.edu.cn

***Abstract*—The rapid development of power system necessitates increasingly critical fault and stability analysis. However, performing such analysis on actual systems is highly challenging, making detailed transient analysis of fault processes using power system simulation software essential. Two established simulation methods are employed: electromechanical transient simulation, focusing on electromechanical dynamics, and electromagnetic transient (EMT) simulation, emphasizing detailed transients. Electromechanical simulation utilizes power flow solutions for rapid initialization. Achieving a consistent steady-state operating point in EMT simulation matching this power flow solution is crucial for precise subsequent fault and stability studies, but is often hindered by complex model structures and parameters within EMT tools. This study uses power flow solutions from the BPA software as the target operating point, rebuilding the model in PSCAD/EMTDC. Based on improved trajectory sensitivity, it investigates factors influencing generator steady-state operation and establishes parameter tuning principles for generator controllers to achieve the target point.**

Keywords—Target Operating Point, Generator, Controller, Trajectory sensitivity

I. Introduction

With the rapid development of power system, the application scenarios of electromechanical transient simulations for quick power flow solutions and electromagnetic transient simulations for precise transient process modeling have expanded significantly[1-2]. PSD-BPA, a mature EMT simulation software, excels in solving system power flows, while PSCAD, an established electromagnetic transient software, demonstrates superiority in analyzing transient processes caused by various faults.

This work was supported by the National Natural Science Foundation of China under Grant U23B6008 and the Science and Technology Project of State Grid Corporation of China under Grant 5100-202455012A-1-1-ZN. (Research and development of an automatic construction platform for electromagnetic transient steady-state operating points in large power grids)

In current electromagnetic transient simulations, when the case topology is complex, component types are diverse, or the research focus is not on generator terminals, the generator is often equivalent to a voltage source with impedance[3]. Detailed modeling is only adopted when generators are the research object, typically connected to an equivalent infinite bus[4]. This approach is unreasonable for actual system modeling—using a complete generator model can make experimental results closer to reality when studying the transient characteristics of a complete system under faults. Reference [5] investigates the mechanism of commutation failure at the receiving end caused by sending end system oscillations based on the CIGRE-HVDC system in PSCAD, where the AC side uses a power source model. Reference [6] proposes a fast initialization method for new energy units and control structures, but the AC side employs an equivalent power source rather than a generator model with control structures.

It is now common to use software like BPA to quickly obtain power flow solutions as target operating points, then establish electromagnetic transient models or use electromagnetic transient software like PSCAD to build identical models for accelerated initialization or transient analysis[7-9], facilitating subsequent transient studies. Reference [10-11] study the conversion of generator models from BPA to PSCAD, but they do not analyze the difference parameters between generator models or the impact of these parameters on operating points.

Therefore, this paper first selects a 9-bus case in BPA as the research background in Section II, setting its power flow solution as the target operating point. To avoid the influence of network topology and transformers, the line and transformer models in the selected case are converted and verified. In Section III, a complete generator model including a speed governor and exciter is constructed. Difference parameters between the two modeling approaches (BPA and PSCAD) are investigated and sorted, and the impact of multiple parameters on the operating point of the PSCAD generator model is analyzed based on the trajectory sensitivity concept. In Section IV, based on the previous research, a mathematical model of the generator's steady-state active power output considering regulators is established. Simultaneously, a parameter tuning method for generators and controllers oriented to target operating points is proposed and verified through case studies.

II. Model Transformation

To establish a case study on the influence of research parameters on steady-state operating points, it is first necessary to conduct model transformation analysis on the main elements of the power grid topology under two methods: transmission lines and transformers.

A. Line Model Transformation and Verification

In BPA, transmission lines usually exist in the form of L card, while in PSCAD, lumped parameter lines can be built through RLC components. The following starts from the L card in BPA and goes to the PSCAD lumped parameter lines to establish the transformation principles of line parameters. The equivalent line transformation is shown in the Fig. 1.

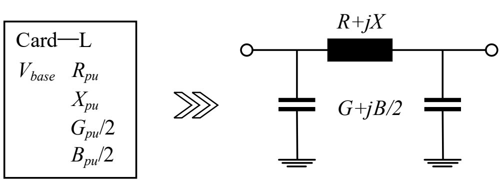

Fig. 1. Transformation from BPA-L Card to PSCAD-RLC Equivalent Line.

BPA usually provides the base capacity, taking S_{base} as the capacity reference and V_{base} as the base voltage, which are given by BPA. The base impedance Z_B of the RLC lumped parameter line in PSCAD can be calculated by (1).

$$Z_B = V_{base}^2 / S_{base} \tag{1}$$

The per-unit values of the RLC lumped parameter lines are also provided by BPA, which are the per-unit value of resistance R_{pu}, the per-unit value of reactance X_{pu}, and the per-unit value of shunt susceptance $B_{pu}/2$ respectively. The per-unit values can be converted into the actual values of resistance, inductance and shunt capacitance in the RLC circuit through the conversion principle given by (2).

$$\begin{aligned} R &= R_{pu} \cdot Z_B \\ L &= X_{pu} \cdot Z_B / (2\pi f) \\ C &= 2\pi f \cdot (B_{pu}/2) / Z_B \end{aligned} \tag{2}$$

f is the base frequency of the RLC lumped parameter lines and is usually set at $50Hz$.

To verify the correctness of the transformation principle, simulation model as shown in Fig. 2 is built in BPA and PSCAD respectively.

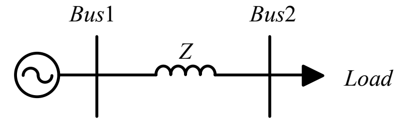

Fig. 2. Single-machine connected load model

Then a series of simulation data are compared, including power flow data of the generator bus and the load bus, as shown in TABLE I. , and TABLE II. . In all the tables mentioned below, P represents active power, Q represents reactive power, δ represents phase angle, and V represents voltage.

TABLE I. Comparison of Generator Bus Power Flow Data

	V (kV)	**δ(°)**	**P(MW)**	**Q(Mvar)**
BPA	230.0	1.5	24.06	0.770
PSCAD	230.1	1.5	24.08	0.778
Difference(%)	0.043	0.0	0.083	1.028

TABLE II. Comparison of Load Bus Power Flow Data

	V (kV)	**δ(°)**	**P(MW)**	**Q(Mvar)**
BPA	228.48	0.35	24.00	9.000
PSCAD	228.60	0.35	24.01	9.004
Difference(%)	0.052	0.00	0.041	0.044

According to the data above, it can be verified that after correct parameter transformation, the L card and RLC components are equivalent in solving steady-state power flow.

B. Transformer Model Transformation and Verification

In BPA, transformers exist in the form of T card, which can be equivalent to the three-phase two-winding transformer in PSCAD. The “Positive sequence leakage reactance” of the transformer in PSCAD corresponds to the “Leakage reactance parameter” in T card, and the “Copper losses” parameter of the PSCAD transformer corresponds to the “Copper loss equivalent resistance” option in T card. Both parameters are per-unit values in the two systems, and the transformation principle is equivalent substitution, which has been verified through multiple simulation experiments.

Using the same way as before, a single-machine connected to load via transformer model as shown in Fig. 3 is built. After simulation, the power flow data of the generator bus and the load bus are compared.

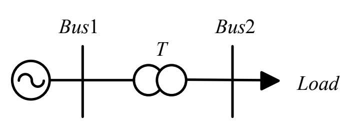

Fig. 3. Single machine connected to load via transformer

The comparison results of bus voltage and bus outlet power flow are shown in TABLE III. and TABLE IV.

TABLE III. BUS VOLTAGE COMPARISON

	Bus1-V(kV)	Bus2- V(kV)
BPA	16.50	227.24
PSCAD	16.51	227.30
Difference(%)	0.006	0.0026

TABLE IV. BUS OUTLET POWER COMPARISON

	Bus1-P (MW)	Bus1-Q (Mvar)	Bus2-P (MW)	Bus2-Q (Mvar)
BPA	24.07	24.00	9.67	9.00
PSCAD	24.08	24.02	9.678	9.004
Difference(%)	0.04	0.08	0.08	0.0044

From above, difference of the operating points under two methods is so small that the T card in BPA and the three-phase two-winding transformer in PSCAD have equivalent substitutability through the above transformation principles. All the work conducted in the following context maintains the equivalence of the model under the two methods.

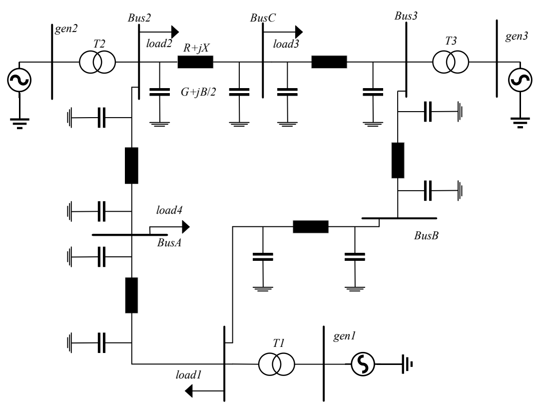

Fig. 4. The topology diagram of 3-machine 9-node system

According to the data provided in BPA, a 3-machine 9-bus model identical to that in BPA is established in PSCAD. The topology of the 3-machine 9-node system is shown in Fig. 4.

In BPA, generators are represented by Bus Card, while in PSCAD, model of "Synchronous Machine" with regulators is built. After completing the model transformation, simulations are conducted to compare the steady-state power flows of generator between BPA and PSCAD. The comparison results are shown in TABLE V.

TABLE V. GENERATOR OUTLET POWER FLOW DIFFERENCES

Line	P(MW)			Q(Mvar)		
	Bpa	*Pscad*	*Difference*	*Bpa*	*Pscad*	*Difference*
gen1-bus1	105.4	107.7	2.18%	43.7	44.1	0.89%
gen2-bus2	163.0	159.4	2.18%	38.6	38.0	1.50%
gen3-bus3	85.0	87.7	3.19%	17.2	17.6	2.27%

From the tables above, it is clear that without research on how to set the parameters in the model of Synchronous Machine and controllers, the steady-state point of the system in two ways demonstrates great difference.

III. MULTI-PARAMETER SENSITIVITY ANALYSIS

In this section, the difference parameters of generators under the two methods are studied for the complete generator system. Then, based on the idea of trajectory sensitivity, the influence of various parameters on the steady-state operating point of the generator is investigated.

A. Generator Differential Parameters and Controller Parameters Summary

First, the difference parameters of generators under the two methods are sorted out in TABLE VI.

TABLE VI. GENERATOR DIFFERENTIAL PARAMETERS

Difference Parameters	Full Name	Description	Value(pu)
MFW	Mechanical friction and windage	Mechanical Damping Constant	0-0.05
NS_{Resist}	Neutral series resistance	Real part of basic frequency impedance connected between neutral point of motor and ground.	Around 10^5
NS_{React}	Neutral series reactance	The imaginary part	Around 0
ILR	Iron loss resistance	Shunt Resistance at Motor Terminals	66.7-300

In BPA, the excitation control can be represented by the EA card. Its inputs are the generator terminal voltage V_T and the reference voltage V_{ref}, and the output is the excitation voltage E_f. The control structure is shown in Fig. 5.

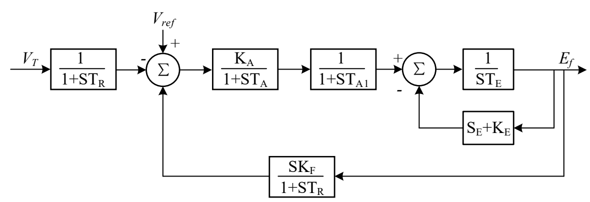

Fig. 5. Excitation Control Structure

In BPA, the speed governing control can be represented by the GH card. Through mathematical adjustment, this model can be converted into the domestic classic speed governing control model, whose control block diagram is shown in Fig. 6. It can be seen that under this control structure, the inputs are the angular velocity unbalance and μ_0, and the output is P_T.

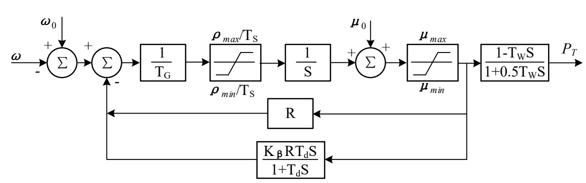

Fig. 6. Typical Speed Governing Control Structure

From the above control block diagram, it can be concluded that in the steady-state, the controller output P_T should be equal to the input μ_0.

B. Parameter Analysis Based on Trajectory Sensitivity

Trajectory sensitivity refers to the sensitivity of the system state trajectory to parameter changes. In this section, using the idea of trajectory sensitivity, the influence of changes in the values of various parameters on the steady-state operating point of the generator is studied respectively. The data for sensitivity analysis are all steady-state curve data.

The expression of trajectory sensitivity is shown in (3). The trajectory sensitivity of parameter x_i refers to the ratio between the change of system output variables and that of x_i.

$$\frac{\partial y(x_i,k)}{\partial x} = \lim_{\Delta x_i \to 0} \frac{1}{\Delta x_i} \cdot \left[y(x_i + \Delta x_i, k) - y(x_i, k) \right] \qquad (3)$$

Through studying the trajectory sensitivity of the difference parameters, as well as the internal control parameters and input parameters of the regulator, to the steady-state operating point of the generator, this paper summarizes the strongly and weakly correlated parameters that cause the offset of the generator's target operating point. Subsequent studies will focus on the strongly correlated parameters. The research is carried out in the 3-machine 9-bus system.

The parameter classification steps are as follows:

1) Set the parameters under study as the lower limit according to the upper and lower limits of parameter floating, and set the remaining parameters as their original values. Sample the steady-state simulation values of voltage, phase angle, active power, and reactive power, and calculate various difference. Equation (4) shows the calculation method for various difference and sensitivity of each parameter.

$$\begin{cases} E_V = \sqrt{\sum_{i=1}^{N} (V_{t,i} - V_{t,i'})^2} \\ E_\delta = \sqrt{\sum_{i=1}^{N} (\delta_{e,i} - \delta_{e,i'})^2} \\ E_P = \sqrt{\sum_{i=1}^{N} (P_{e,i} - P_{e,i'})^2} \\ E_Q = \sqrt{\sum_{i=1}^{N} (Q_{e,i} - Q_{e,i'})^2} \end{cases} \rightarrow \begin{cases} S_{V,i} = \sum_{m=1}^{M-1} \left| E_{V,i,m+1} - E_{V,i,m} \right| \\ S_{\delta,i} = \sum_{m=1}^{M-1} \left| E_{\delta,i,m+1} - E_{\delta,i,m} \right| \\ S_{P,i} = \sum_{m=1}^{M-1} \left| E_{P,i,m+1} - E_{P,i,m} \right| \\ S_{Q,i} = \sum_{m=1}^{M-1} \left| E_{Q,i,m+1} - E_{Q,i,m} \right| \end{cases} \qquad (4)$$

In the right equation, E is the difference, $V_{t,i}$ is the voltage sampling data under the original parameter values and $V_{t,i'}$ is the voltage sampling data after changing the parameter x_i. In the left equation, $S_{V,i}$ is the voltage sensitivity index of the parameter, and other parameters follow the same notation, while $E_{V,i,m}$ is the voltage error of parameter x_i at the m-th variation step of parameter and M is the total number of parameter variation steps.

2) Perform simulations for the next step increment according to the parameter variation step size, calculate various errors in Step 1), save the errors, and repeat Step 2) until the parameter reaches its upper limit.

3) The sensitivity of each parameter is measured by the sum of absolute values of numerical changes within a unit step, as shown in the right equation of (4).

After determining the value range of each type of parameter and the corresponding step size H for each parameter, the sensitivity of each type of parameter to the operating point was calculated, and the results are shown in TABLE VII. To facilitate data presentation, the table is divided into four parts by parameter type, which are, from top to bottom, difference parameters, excitation control internal parameters, speed regulation control internal parameters, and controller input parameters.

TABLE VII. SENSITIVITY ANALYSIS OF MULTIPLE PARAMETERS TO STEADY-STATE OPERATING POINT

	Range	H	V	δ	P	Q
MFW	0-0.05	0.005	0.001	0.82	7.66	1.01
NS_{Resist}	$0\text{-}10^9$	10^n	0	0	0	0
NS_{React}	$0\text{-}10^9$	10^n	0	0	0	0
ILR	0-300	20	0	0.246	2.28	0.3
TR	0-0.06	0.004	0	0	0	0
KA	25-400	25	0	0.001	0	0.03
TA	0.02-0.2	0.02	0	0	0	0.01
KF	0.01-0.1	0.01	0.003	0.032	0	0.29
TF	0.1-1	0.1	0.002	0.005	0	0.06
TE	0.1-0.5	0.1	0	0.004	0	0.01
1/TG	1.0-10.0	1	0	0	0	0
Td	2.5-27.5	2.5	0	0	0	0
Tw	0.5-5	0.5	0	0	0	0
Dd	0.1-1	0.1	0	0	0	0
R	0.03-0.06	0.003	0	0	0	0
Vref	1.0-1.1	0.01	0.01	0.099	1.53	0.76
μ0	0.8-0.9	0.01	0.01	0.001	1.65	15.3

The results show that the sensitivities of the aforementioned parameters to the steady-state voltage basically remain around 0, indicating that their impact on the steady-state voltage of the generator is negligible within a reasonable range. With respect to the phase angle, MFW and ILR exhibit the highest and second-highest sensitivities, respectively, while the sensitivities of other parameters hover around 0 and can be neglected.

For the active power P, MFW, ILR, μ_0, and V_{ref} exhibit relatively high sensitivities in descending order. The sensitivities of other parameters remain exactly at 0, which means that variations in these parameters do not affect the active power output of the generator under steady-state conditions. Regarding the reactive power Q, μ_0 exhibits an extremely high sensitivity, followed by V_{ref}. Additionally, ILR and KF also exhibit higher sensitivities compared to other parameters. It can conclude that:

1) Within the value ranges of difference parameters, changes in MFW and ILR can cause shifts in the operating point of Generator, while NS_{Resist} and NS_{React} have negligible influence on the operating point.

2) Changes in internal controller parameters have nearly no impact on the steady-state operating point.

3) Inputs to the excitation control play a dominant role in causing voltage, phase angle, and reactive power shifts.

4) Inputs to the speed governing control play a dominant role in causing phase angle and active power shifts.

IV. Steady-State Active Power Output Model of Generator Considering Regulators

Based on the findings from previous section that identified the main influencing factors of the generator's steady-state operating point, this section establishes a steady-state active power output model of the generator considering regulators according to the definitions provided in PSCAD. Meanwhile, the tuning principle of controller parameters is proposed and verified through case studies.

A. Theoretical Loss Models

As indicated by the trajectory sensitivity analysis in Section III, without changing the network topology or load, the primary factor affecting the generator's steady-state terminal voltage is the input of the excitation control. Therefore, for the voltage component in the target operating point, the excitation control input reference voltage can be set according to the power flow calculation results. The following analysis focuses on the generator's steady-state active power output.

Under ideal conditions, the input torque T_m of generator, input of speed control μ_0 and active power of generator P_g have a relationship expressed by (5) when $\omega=\omega_0$ in steady-state.

$$T_m = \mu_0 \rightarrow P_m = T_m \cdot \omega_0 \rightarrow P_g = P_m \tag{5}$$

However, in practical scenarios, parameters that may introduce losses in the considered generator model include the stator resistance R_a, as well as the parameters MFW and ILR analyzed in the preceding text. The loss models for these three parameters are provided in TABLE VIII. according to their definitions.

TABLE VIII. Theoretical Loss Models for the Parameters

Parameter	Loss Model theory	Loss Model
Ra	Related to the square of the current	$P_{Ra}=Ia^2 \cdot Ra$
MFW	Fixed value	$P_{MFW}=K \cdot MFW$
ILR	Related to the square of terminal voltage	$P_{ILR}=V^2/ILR$

Based on the loss models provided above, the theoretical steady-state active power output model of the generator can be derived, as expressed by (6).

$$\begin{aligned} P_g &= P_m - P_{MFW} - P_{Ra} - P_{ILR} \\ &= T_m \cdot \omega_0 - K \cdot MFW - I_a^2 \cdot R_a - \frac{V^2}{ILR} \\ &= u_0 - K \cdot MFW - I_a^2 \cdot R_a - \frac{V_{ref}^2}{ILR} \end{aligned} \tag{6}$$

B. Validation of Loss Model and Active Power Output Model of Generator

The value of MFW was changed in equal steps within the range from 0 to 1 with a step size of 0.05. Multiple simulations were conducted, and relationship between P_g and MFW was fitted using linear and polynomial methods. The regression analysis results yielded the regression curves as shown in Fig. 7.

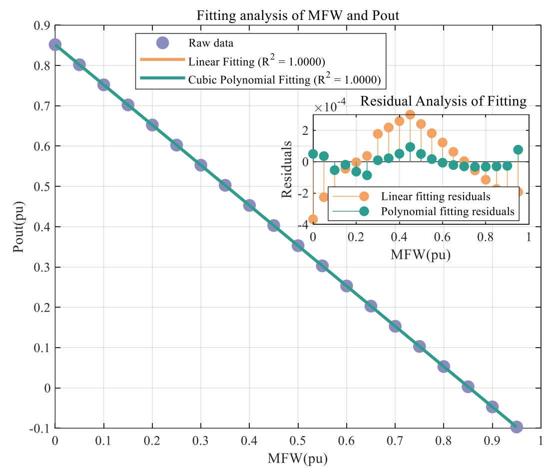

Fig. 7. Fitting Results

As shown above, both the linear and polynomial regression curves closely match the original data, yielding the linear relationship of P_g=0.852-0.999MFW. It confirms that MFW introduces active power losses equivalent to the value itself in the generator's steady-state active power output, and K in the MFW loss model is determined to be 1.

For the parameter ILR, since it is defined as the terminal shunt resistance and its loss model is related to the square of the voltage, the difference relationship of generator active power output for any two ILR values is shown in (7).

$$\frac{U^2}{ILR_1} - \frac{U^2}{ILR_2} = P_{g2} - P_{g1} = \Delta P \tag{7}$$

Difference on the left side can be obtained by measuring the terminal voltage and combining it with ILR, serving as theoretical value. Difference on the right side can be obtained by measuring the active power of generator, which is simulation value. The correctness of the ILR loss model can be verified by comparing the curves of the theoretical and simulation values. Similarly, simulations are conducted by changing ILR values in equal steps. The result is shown in Fig. 8. Meanwhile, the difference between two curves is also displayed.

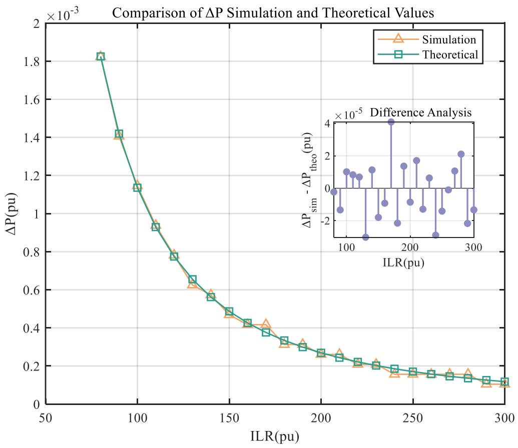

Fig. 8. Comparison Between Simulation Curve and Theoretical Curve of ΔP

As shown in Fig. 8, there is a slight difference between simulation curve and theoretical curve of ΔP. Meanwhile, the absolute value of the difference between the two curves in the inset is within the range of 10^{-4} to 10^{-5}, which is acceptable. The above experiments verify the loss model of ILR.

To validate the generator steady-state active power output model corresponding to (6), the stator resistance R_a and parameter MFW are first excluded by setting 0 value, transforming (6) into the form of (8).

$$\frac{V^2}{ILR} = \mu_0 - P_g \tag{8}$$

The left side of (8) is processed in the same way as before, obtained by measuring the terminal voltage and combining it with the ILR setting value, serving as the theoretical value of the power difference. The right-side difference can be obtained by measuring the controller input μ_0 and the generator outlet active power P_g, serving as the simulation value of the power difference. Similarly, simulations are conducted by changing the ILR values in equal steps within the value range. The comparison curves are shown in Fig. 9.

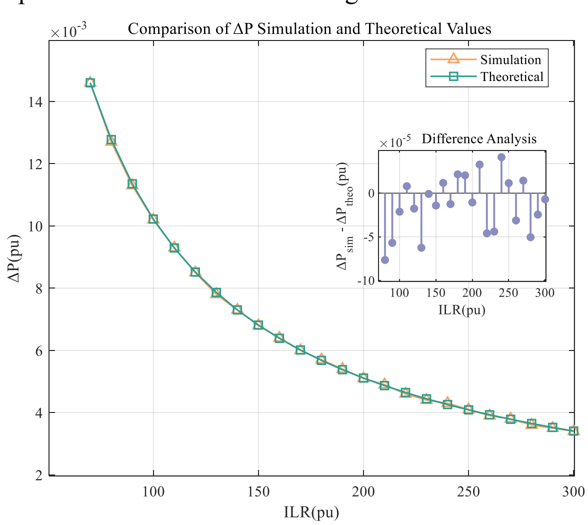

Fig. 9. Comparison Between Simulation Curve and Theoretical Curve of ΔP

The two curves in Fig. 9 basically coincide, and the curve difference displayed in the inset is within the range of 10^{-4} to 10^{-5}, which is acceptable. Therefore, the generator steady-state active power output model without considering the stator resistance R_a is verified.

To validate the loss model of stator resistance R_a, the MFW parameter is first excluded, transforming (6) into (9).

$$I_a^2 \cdot R_a = T_m - P_g - \frac{V^2}{ILR} \tag{9}$$

Following the previous approach, after measuring the current and combining it with the set stator resistance R_a, the theoretical power difference is calculated, while the right side of the formula represents the simulation power difference. The result of curve comparison is shown in Fig. 10.

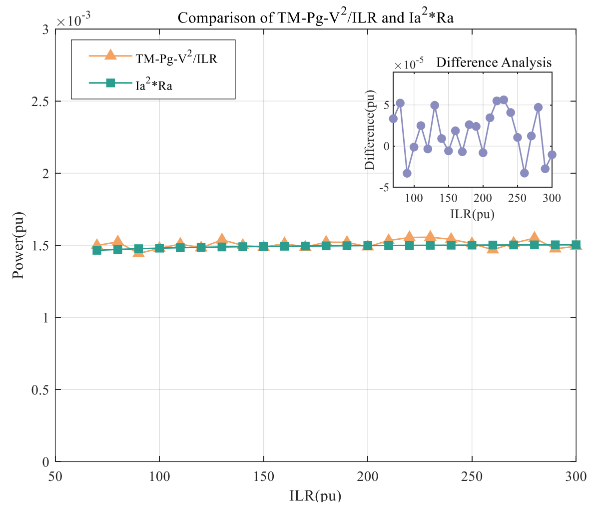

Fig. 10. Comparison Between Simulation Curve and Theoretical Curve of ΔP

As shown in Fig. 10, the two curves basically coincide, and the curve difference is also within the range of 10^{-5}, which is acceptable, verifying the loss model of R_a.

Through the above research, the steady-state active power output model of the generator under the determined controller input and difference parameter setting is given, and the specific model is shown in Fig. 11.

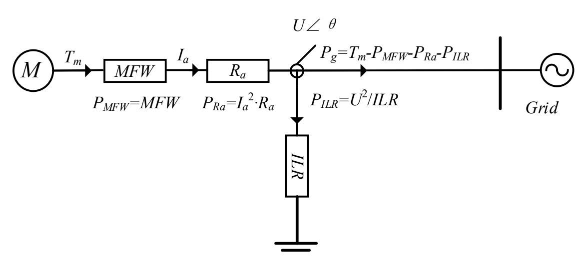

Fig. 11. Steady-State Active Power Output Model of Generator

C. Measurement Difference Analysis and Controller Parameter Tuning

Based on the previous research, when R_a is not considered, the steady-state active power output of the generator can be determined according to the controller input under system stability. The following research focuses on how to set the controller input to make generator reach target operating point.

First, attempt to use P_0 as the input to the speed governor and V_0 as the input to the excitation control. The data derived from the BPA power flow solution provides the target operating point, yielding the operating point comparison shown in TABLE IX.

TABLE IX. OPERATING POINT COMPARISON

	V(pu)	Delta(°)	P(Mw)	Q(Mvar)
BPA	1.01	5.09	163.00	38.60
PSCAD	1.01	4.63	162.15,159.25	38.05

In the table, there are two sets of data for the active power item corresponding to PSCAD. It is found that this is caused by inconsistent sources of active power measurement and different active power data under the two measurement methods. The left data is measured by the built-in active power output signal of the synchronous machine model, and the right data is measured by the active power signal of the Multimeter component connected in parallel with the generator outlet line. In fact, the active power measured by the Multimeter component should be consistent with the target operating point active power.

To verify whether this measurement difference exists as a constant value in a specific system, parameters are also changed in equal steps to obtain active power data under the two measurement methods for analysis. The comparison of active power data between the two methods is shown in Fig. 12, where P_g is measured by the built-in active power output signal of the synchronous machine model, and P_{out} is measured by the active power signal of the Multimeter component connected in parallel with the generator outlet line.

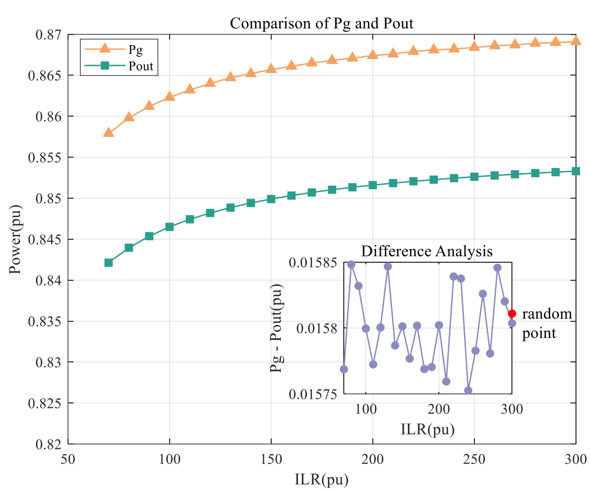

Fig. 12. Active Power Comparison from Divergent Measurement Sources

As shown in Fig. 12, this measurement difference approximately exists in the system as a constant value of 0.0158. To further verify its correctness, random difference parameters and stator resistances are assigned to the generator to obtain measurement errors under specific working conditions (i.e., the random point in Fig. 12), which also falls within the difference interval.

According to the above analysis, it can be concluded that this difference exists as a constant value in the steady state. If the active power measured between the generator outlet and the connected bus is taken as the operating point, a parameter tuning method for the target operating point without considering the stator resistance can be proposed based on previous research. The process is shown in Fig. 13, and this parameter tuning method is a linearization method.

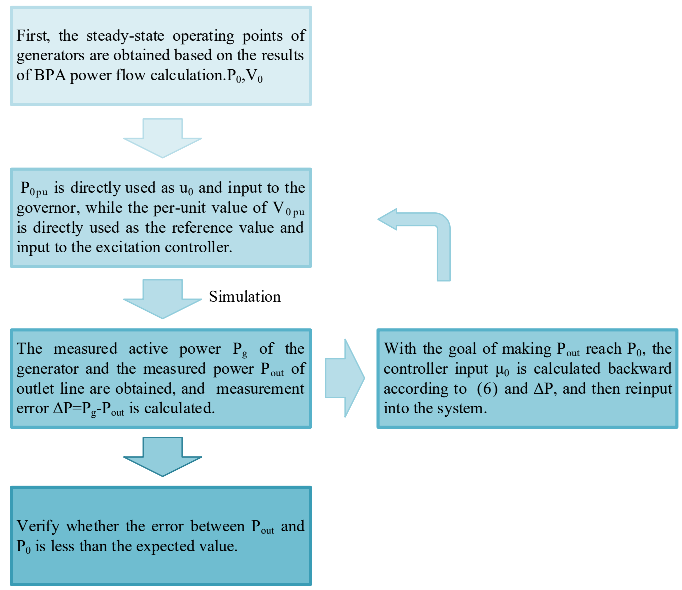

Fig. 13. Parameter Tuning Method without Considering Stator Resistance

According to the above tuning method, the controller inputs are redetermined, and the generator operation results under this condition are compared with the target operating point. The results are shown in TABLE X.

TABLE X. COMPARISON OF OPERATING POINTS AFTER TUNING

	V(pu)	δ(°)	P(Mw)	Q(Mvar)
BPA	1.01	5.09	163.0	38.60
PSCAD	1.01	5.04	162.9	38.57

When R_a is considered, different controller inputs will lead to inconsistent steady-state currents of the generator, and the controller input and the active power of the operating point show a nonlinear correlation. In this case, using the above global linearization parameter tuning method to back-calculate the controller input will cause a large difference between the generator steady-state operating point and the target operating point. Therefore, a parameter tuning method based on local linearization can be used for controller parameter tuning.

The specific steps are as follows: taking the target operating point as the center of parameter tuning, dividing the boundary of 0.05pu on both sides, carrying out simulation in equal steps, determining the step interval to which the target operating point belongs based on the simulation results, linearizing the corresponding interval, obtaining the linearized equation between the controller input and the active operating point, and substituting the target operating point to back-calculate the controller input.

In the verifying case, R_a is set to 0.002pu, and the steady-state operating points under the target operating point, the controller input obtained by the global linearization parameter tuning method, and the controller input obtained by the linearization of the simulation interval considering nonlinearity are compared. The comparison results are shown in TABLE XI.

TABLE XI. COMPARISON OF OPERATING POINTS OF DIFFERENT WAYS

	V(pu)	δ(°)	P(MW)	Q(Mvar)
BPA	1.01	5.09	163.0	38.60
Global Linearization	1.01	5.01	162.7	38.52
Interval Linearization	1.01	5.04	162.9	38.57

It can be seen that when R_a is very small, there is a large deviation between the operating point after global linearization parameter tuning and the target operating point, while the operating point after interval linearization parameter tuning is very close to the target operating point. This proves the rationality of the interval linearization parameter tuning method after considering the nonlinear relationship between the controller input and the operating point caused by the presence of R_a.

V. CONCLUSION

This study conducts research based on electromechanical transient simulation software BPA and electromagnetic transient simulation software PSCAD. Taking the BPA power flow calculation results as the generator's target operating point, the research investigates how to achieve this target operating point for a complete generator system with regulators in the PSCAD environment.

The methodology involves three main phases:

1) First, equivalent transformation of network topology is implemented. Second, parameters of typical generator controllers and the difference parameters of generator models under two operational modes are systematically examined.

2) Subsequently, employing the concept of trajectory sensitivity, the influence of internal controller parameters, input parameters, and generator model difference parameters on steady-state operating points in PSCAD is analyzed, identifying strongly correlated parameters that dominantly affect operating points. Based on these parameters, corresponding loss models and active power output models under steady-state conditions are developed and validated through case studies.

3) Finally, leveraging preceding findings, this paper proposes two parameter tuning principles: one considering stator resistance and another disregarding it. Case verification demonstrates the effectiveness of both tuning strategies.

This comprehensive study on the steady-state output characteristics of generators in PSCAD provides guidance for electromagnetic transient modeling based on actual power system.

ACKNOWLEDGMENT

This work was supported by the National Natural Science Foundation of China under Grant U23B6008 and the Science and the Technology Project of State Grid Corporation of China under Grant 5100-202455012A-1-1-ZN.(Research and development of an automatic construction platform for electromagnetic transient steady-state operating points in large power grids).

REFERENCES

[1] Y. Liu, M. Zou, Y. Wang, M. Feng, J. Xu, X. Jia and C. Zhao, "Equivalent modeling method for electromagnetic transient of permanent magnet synchronous generator for offshore wind power simulation," Transactions of China Electrotechnical Society, vol. 39, no. 8, pp 2400-2411, 2024.

[2] S. Cao, J. Xu, Y. Zhou, H. Chen and M. Feng, "Electromagnetic transient fine-grained parallel simulation method applicable to large-scale photovoltaic power stations," Transactions of China Electrotechnical Society, pp. 1-14, 2025.

[3] X. Wu, L. Zhao, B. Zhou, C. Hong, Y. Su and S. Tu, "Steady-state initialization of AC-DC grids with complex controllers for transient simulations," 2022 4th International Conference on Smart Power & Internet Energy Systems, Beijing, 2022, pp. 1523-1527.

[4] A. Chitransh, S. Kaur and R. Parveen, "Comparative analysis of different configuration of generators for extraction of wind energy," 2021 Fifth International Conference on I-SMAC, Palladam, 2021, pp. 1765-1773.

[5] L. Zheng, J. Wu, Y. Xu, Y. Sun and C. Liu, "Mechanism analysis of receiving end commutation failure caused by sending end oscillation in HVDC transmission system," Transactions of China Electrotechnical Society, vol. 39, no. 9, pp. 2743-2754, 2024.

[6] J. Ocampo-Wilches, J. Mahseredjian, K. Jacobs, A. Pavani and H. Xue, "Comprehensive full-scale converter wind park initialization for electromagnetic transient studies," IEEE Transactions on Power Delivery, vol. 40, no. 3, pp. 1459-1468, 2025.

[7] Y. Dong, J. Guo, S. Miao, J. Hou, J. Han and S. Ma, "A novel electromagnetic transient simulation method of large-scale AC power system with high penetrations of DFIG-based wind farms," IEEE Access, vol. 10, pp. 53188-53199, 2022.

[8] S. Mu, H. Wang, T. Liu, X. Li, H. Dai and X. Xiao, "Initialization of DFIG wind turbine for electromagnetic transients simulation," 2021 International Conference on Power System Technology, Haikou, 2021, pp. 1-8.

[9] Y. Liu, Y. Song, L. Zhao, Y. Chen and C. Shen, "A general initialization scheme for electromagnetic transient simulation: towards large-scale hybrid AC-DC grids," 2020 IEEE Power & Energy Society General Meeting, Montreal, 2020, pp. 1-5.

[10] B. Cao, S. Yuan, Q. Wang, Y. Cong and Y. Liu, "Research on automatic conversion technology of power grid model from PSD-BPA to PSCAD," Inner Mongolia Electric Power, vol. 38, no. 04, pp. 1-8, 2020.

[11] H. Tao, J. Xu and W. Zou, "Research on model conversion from BPA to PSCAD," Electric Power Automation Equipment, vol. 33, no. 08, pp. 152-156, 2013.